Self-Probing Spectroscopy of the SF 6 Molecule: A Study of the Spectral Amplitude and Phase of the High Harmonic Emission

Bastian Manschwetus, Nan Lin, Jan Rothhardt, Roland Guichard, Thierry Auguste, Antoine Camper, Pierre Breger, Jérémie Caillat, Marie Géléoc, Thierry Ruchon, et al.

Self-probing spectroscopy of the SF_6 molecule: a study of the spectral amplitude and phase of the high harmonic emission

Bastian Manschwetus,[*,†,¶] Nan Lin,[†,§] Jan Rothhardt,[†,‖] Roland Guichard,[‡] Thierry Auguste,[‡] Antoine Camper,[‡] Pierre Breger,[‡] Jeremie Caillat,[‡] Marie Géléoc,[†] Thierry Ruchon,[†] Richard Taïeb,[‡] Bertrand Carré,[†] and Pascal Salières[†]

CEA-Saclay, IRAMIS, Laboratoire Interactions, Dynamique et Lasers, 91191 Gif-sur-Yvette, France, and UPMC Univ. Paris 06, UMR 7614, Laboratoire de Chimie Physique-Matière et Rayonnement, 11 Rue Pierre et Marie Curie, 75231 Paris Cedex 05, France

E-mail: bastian.manschwetus@fysik.lth.se

[*]To whom correspondence should be addressed

[†]CEA-Saclay, IRAMIS, Laboratoire Interactions, Dynamique et Lasers, 91191 Gif-sur-Yvette, France

[‡]UPMC Univ. Paris 06, UMR 7614, Laboratoire de Chimie Physique-Matière et Rayonnement, 11 Rue Pierre et Marie Curie, 75231 Paris Cedex 05, France

[¶]Department of Physics, Lund University, PO Box 118, SE-22100 Lund, Sweden

[§]Laboratorium für Physikalische Chemie, ETH Zürich, Wolfgang-Pauli-Strasse 10, 8093 Zürich, Switzerland

[‖]Helmholtz-Institute-Jena, Fröbelstieg 3, 07743 Jena, Germany

Abstract

We present characterizations of the attosecond pulse train produced in the high harmonic generation (HHG) from SF_6 molecules irradiated by strong pulsed laser field at 800 nm. At harmonic order 17, we observe a minimum in the amplitude of the emitted spectrum and a corresponding distortion in the phase. Our experimental results are compared to two models: a multi-center interference model focused on the effect of the structure of the SF_6 molecule in HHG and a model focused on the interferences between multiple ionization channels in HHG. We find that the experimental results agree very well with the multiple ionization channels model, illustrating that HHG in molecules can be very complex and that it provides insights of the intra-molecular electron dynamics during the interaction process.

1 Introduction

Since the discovery of high harmonic generation (HHG) in gas medium,[1,2] its capacity to generate attosecond pulse trains[3] and single attosecond pulses[4] has opened the way to study molecular structures and dynamics of molecular bound states and continuum states on a sub-femtosecond time scale.[5] The success of HHG-based time-resolved experiments relies notably on a fairly simple model describing the HHG itself in three steps, at the single atom/molecule level.[6,7] In this model the atom or molecule is ionized by a tunnel process through the potential barrier formed by the interaction of the atomic coulomb potential with the strong laser field. After ionization, the free electron wavepacket (EWP) in the continuum is accelerated in the oscillating laser field. For linear laser polarization the EWP may be then driven back to the ion and finally recombine with the ion. The excess energy of the electron is then emitted as a XUV photon. For sinusoidal laser fields, the three-step sequence is repeated periodically every half cycle, resulting in the emission of coherent, attosecond, bursts of XUV pulses – composed of odd harmonics of the driving IR field. The photon energies depends on the laser intensity and wavelength as well as on the ionization

potential of the target atom or molecule; for Titanium:Sapphire lasers at approximately 800 nm wavelength photon energies up to 1 keV can be achieved,[8] for an infrared source of 3.9 µm wavelength the generation of coherent x-rays up to 1.6 keV energy has been reported.[9]

The HHG process, i.e., the inelastic scattering of the recolliding electron in the radiative channel, can also serve as a probe to investigate both the structure and dynamics of the emitting target, a technique now referred to as high harmonic spectroscopy. The time and space resolutions of this probe are determined by the properties of the recolliding continuum electron which encodes the information in the emitted XUV light bursts. The whole process takes place within one half cycle of the laser field, which is 1.3 fs for an 800 nm laser source. This allows probing electron or nuclear dynamics with an attosecond time resolution.[10] The spatial resolution of the recolliding electron probe is given by its de-Broglie wavelength, which is of the order of 1 Å, similar to the size of small molecules for typical electron kinetic energies of several 10 eV.[11] These unique characteristics of the HHG process open new possibilities to investigate atoms and molecules. For example nuclear and electronic dynamics after rotational,[12] vibrational[13] or dissociative excitation[14,15] where studied using their influence on the HHG process.

In the harmonic emission from molecules characteristic features, for example spectral minima,[12,16] phase shifts[11] or polarization changes are observed.[17,18] For their interpretation, usually two routes have been studied in the past, either the influence of the molecular structure on the HHG, allowing for example the tomographic reconstruction of the emitting orbital,[11,19,20] or the HHG from multiple ionization channels, probing the charge dynamics on the attosecond timescale inside the molecule.[10] But also a combination of the two is possible, and which interpretation is the most adapted has to be considered thoroughly for each specific experiment. For the HHG in SF_6, a recent article indicates that multiple interfering ionization channels are contributing to the process.[21]

In this article, we investigate thoroughly the spectral amplitude and phase of the attosecond emission generated by SF_6 molecules irradiated by femtosecond pulses with 800

nm wavelength. The article is structured in five different sections. In Section 2, we will describe briefly our experimental setup and the spectral phase measurements with the RABBIT method. We then present the experimental results in Section 3. The influence of the phasematching in the macroscopic gas medium is discussed in Section 4. Two different models are developed to interpret the results. The model in Section 5 emphasizes the structural interference within a single ionization channel of the SF_6 molecule and the model in Section 6 emphasizes interferences arising in HHG from multiple ionization channels.

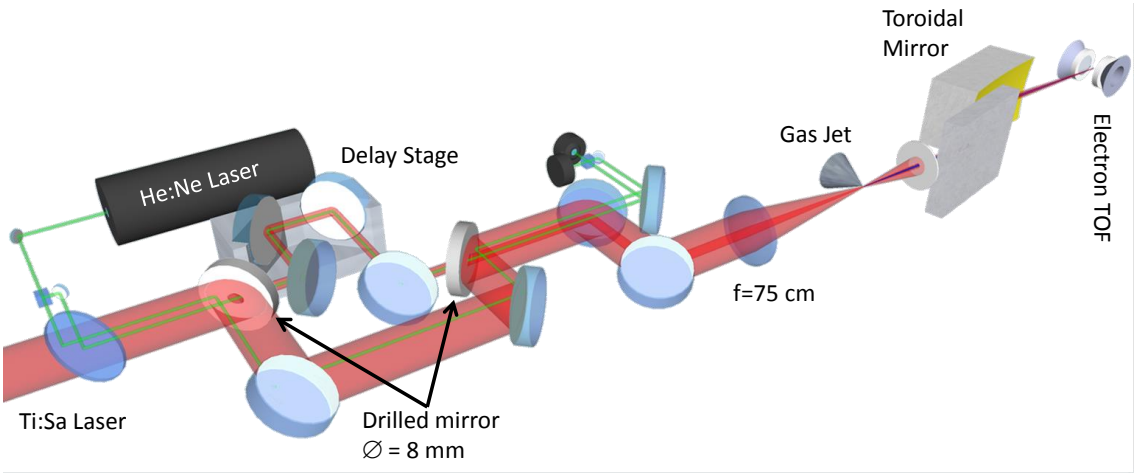

Figure 1: Schematics of the optical setup for the RABBIT measurements, see text for explanation.

2 Experimental setup

The experimental setup is made of two main parts, first HHG in a SF_6 or Ar gas jet, and second the characterization where spectral amplitude and phase of the attosecond emission are measured with the RABBIT technique. The RABBIT method makes use of the two-color photoionization of a rare gas target by the XUV radiation in the presence of a weak infrared "dressing" field.[3] When the IR dressing field is synchronized with the XUV comb (atto pulse train), new satellite lines or sidebands appear in the photoelectron spectrum at the energies of even orders of the fundamental IR. In the RABBIT regime, these sidebands are

mainly populated through two interfering quantum paths: absorption of one XUV photon of (q-1)th harmonic plus one IR photon (at frequency ω_0), or absorption of one XUV photon of (q+1)th harmonic and stimulated emission of one IR photon.[22] The attosecond beating between two neighboring harmonics is thus revealed by scanning the delay between the XUV comb and the dressing IR. The phase of the sidebands oscillations at $2\omega_0$ gives access to the group delay or emission time of the attosecond emission. An additional atomic phase factor coming from the photoionization process can safely be neglected in the further discussion.[23] By integrating the differential phase over the whole spectrum the spectral phase of the "average" single attosecond pulse in the train can be retrieved. In HHG, in the simplest case of a dominant channel, this spectral phase is usually decomposed as the phase accumulated by the free EWP in the continuum, plus the phase acquired in the recombination, appearing as the argument of the corresponding complex dipole. The spectral variations of the phase encodes as well information about possible sub-fs multi-orbital dynamics occurring in the molecule. This information can be extracted from the data when the continuum phase and recombination dipole phase for all contributing ionization channels are known.

The experiments were performed at the PLFA Laser Facility of the CEA-Saclay. The laser system delivers 13 mJ pulses of 40 fs pulse length with a repetition rate of 1 kHz. The central wavelength of the laser is 804 nm. An overview of the experimental setup is shown in Figure 1, a detailed description may be found here.[24] The high harmonic radiation was generated by focusing laser pulses of 0.6 to 1.5 mJ energy into a pulsed supersonic gas jet of SF_6 or argon with a nozzle diameter of 200 µm, reaching peak intensities in the focal spot of 0.6×10^{14} Wcm^{-2} to 1.1×10^{14} Wcm^{-2}. The backing pressure of the gas jet was chosen between 1.5 bar and 4 bar. After the harmonic generation, the XUV light is refocused into the detection area of magnetic bottle spectrometer, where it crosses an effusive jet of argon gas and produces photoelectrons. From their time of flight the photoelectron energy spectrum is calculated. For implementing the RABBIT technique, we used a Mach-Zehnder interferometer using drilled mirrors before the HHG. It splits the incoming laser

beam into a strong annular beam for the HHG and a weak central beam for the XUV-IR cross correlation. The path-length difference of the two interferometer arms is controlled with sub-10 nm precision by a piezo actuator and actively stabilized by copropagating a green He-Ne laser beam in each arm.

3 Results

With our experimental setup we measured the complex spectrum (intensity and phase) for the harmonic orders 11 to 27 generated in SF_6 for three different generation laser intensities 0.6×10^{14} Wcm^{-2}, 0.7×10^{14} Wcm^{-2} and 1.1×10^{14} Wcm^{-2} at a backing pressure of 3 bar and for six backing gas pressures between 1.5 bar and 4 bar at a laser intensity of 1.1×10^{14} Wcm^{-2}. For each set of conditions we took a RABBIT spectrogram ("scan"), the photoelectron spectrum versus the delay between the IR pulse and the XUV attosecond pulse train, within a range of 30 fs around zero delay; a typical scan is shown in Figure 2 a). The overall signal of SF_6 was approximately a factor 50 smaller than the signal from argon, really pushing our signal to noise ratio to the limit in the RABBIT scans. In Figure 2 b), we present the intensity of each harmonic order extracted from the RABBIT scan after integrating over the delay axis. The dressing field does not contribute to the ionization of the target gas; it only redistributes the photoelectron energy through free-free transitions. After integration along the delay axis, the intensity of the dressed harmonic peaks is proportional to the intensity of the undressed harmonics, which allows us to extract the spectral shape of the harmonic emission directly from the RABBIT measurement without an additional measurement of the "undressed" HHG, eliminating one possible error source. First, the intensity dependences of the SF_6 and Ar spectra are shown in Figure 2 c). The generation intensity in the focus was estimated by comparing the slope of the measured group delays for Ar (as a function of XUV frequency) to SFA calculations; this estimate was a factor of two lower than the intensity calculated from the generation beam energy and diameter. All XUV

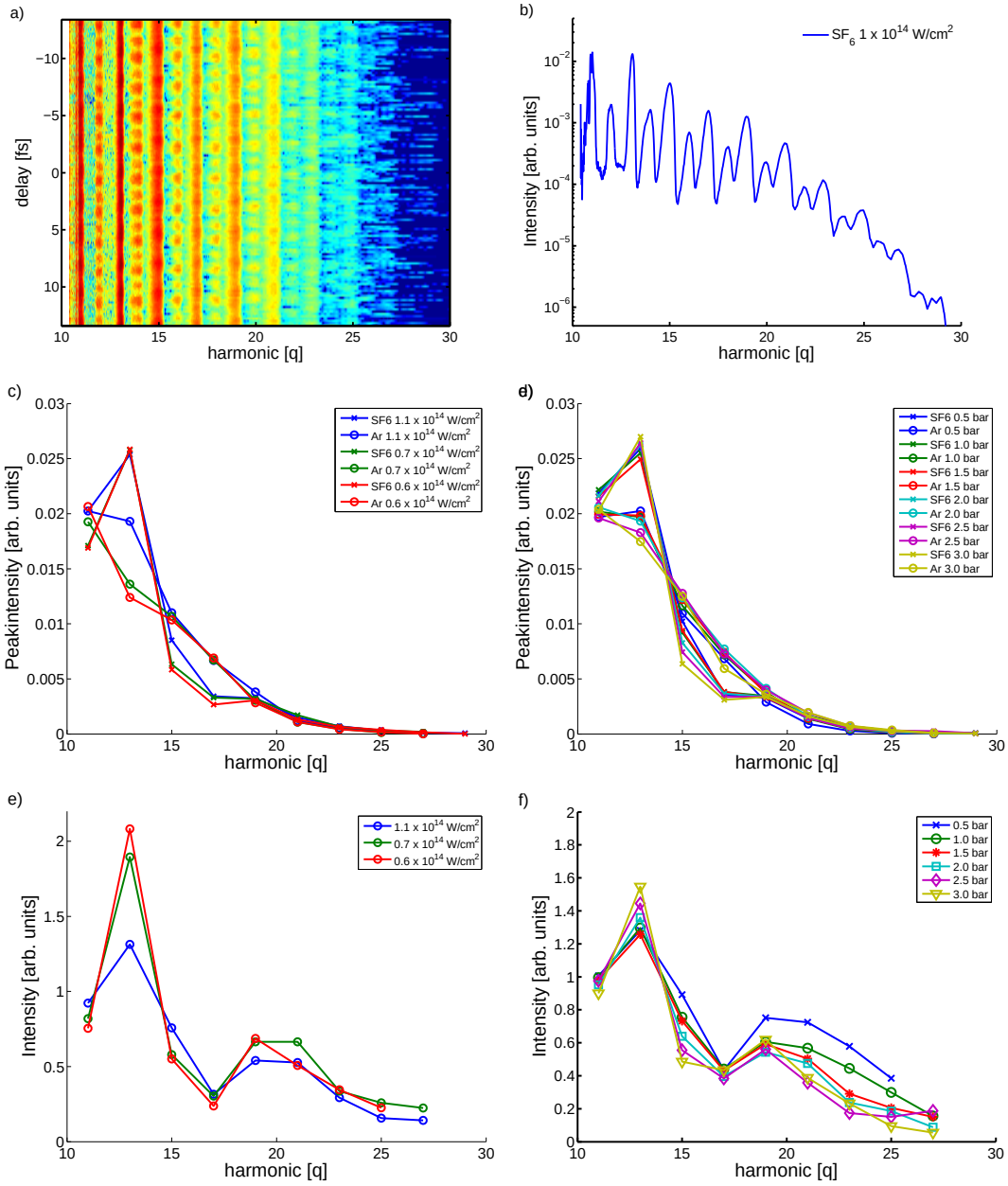

Figure 2: a) RABBIT spectrogram of the high harmonics generated in SF_6 at a laser intensity of 1.1×10^{14} Wcm^{-2} on a logarithmic color scale and b) spectral intensity of the RABBIT spectrogram in a) integrated over the delay. Comparison of the spectral intensities of the high harmonic peaks on a linear scale extracted from different RABBIT scans at c) three generation intensities from 0.6×10^{14} Wcm^{-2} to 1.1×10^{14} Wcm^{-2} and 3 bar backing pressure and d) six backing gas pressures from 1.5 bar to 4 bar at 1.1×10^{14} Wcm^{-2} generation intensity. The spectra are still convoluted with the spectral response of the beam line and the detector. A detailed description of the calibration procedure is given in Section 5. The harmonic spectral intensity of SF_6, calibrated by that in Ar is shown in e) for the three different generation intensities and in f) for the six different gas pressures of the generation medium.

spectra from SF_6 exhibit a very remarkable feature, i.e., a pronounced intensity minimum around the harmonic order 17 (H17), which is not visible in the Ar spectra. All spectra roll off fast in the spectral intensity after H21. For the two close intensities 0.6×10^{14} Wcm^{-2} and 0.7×10^{14} Wcm^{-2} the corresponding spectra either in SF_6 or in Ar are very similar. For intensity of 1.1×10^{14} Wcm^{-2} the H15 in SF_6 is slightly higher than in the previous spectra, the H13 in Ar increases with only small variations at the neighboring harmonic orders. Finally, for increasing generation laser intensity, the observed minimum at H17 in the HHG spectra of SF_6 moves slightly from in between H15 and H17 to directly on H17.

Second, we performed RABBIT measurements at different backing gas pressures (1.5 to 4 bar) of the generation gas, shown in Figure 2 d). In the pressure dependence of the SF_6 spectra, we observe an evolution of the spectral shape mainly at H15, which intensity decreases for the highest gas pressures and drops by roughly a factor two over the whole pressure range. The intensity of the other harmonic orders is approximately independent of the gas pressure. For the Ar HHG spectra, we observe a pressure dependance in the harmonic orders 21, 23, 25 and 27, which all increase with increasing gas pressure. All spectra discussed so far are convoluted with the beamline transmission and the detector response. For calibration of the spectra, we used the Ar HHG spectra taken under the same generation conditions as a reference. In Figure 2 e) and f), we plot the ratio of the intensities measured in SF_6 and in Ar and multiplied by the photoionization cross section Ar. As will be shown in Section 5, under certain assumptions, this calibration also removes, in the total HHG dipole, the spectral dependence of the ionization amplitude and the continuum amplitude (free electron wavepacket), thus greatly simplifying the interpretation of the measurement. Finally we retrieve the calibrated HHG spectral intensity in SF_6; it is shown in Figure 2 e) for three different generation laser intensities 0.6×10^{14} Wcm^{-2}, 0.7×10^{14} Wcm^{-2} and 1.1×10^{14} Wcm^{-2} at a backing pressure of 3 bar and in Figure 2 f) for six backing gas pressures of 1.5 bar to 4 bar at a laser intensity of 1.1×10^{14} Wcm^{-2}. In the generation conditions considered, the spectral response from SF_6 shows a pronounced maximum at H13

followed by a minimum at H15 and H17, which is clearer than in the uncalibrated data. Above H21 the spectral intensity decreases slowly. For the increasing generation intensities, we see a strong decrease of H13 while H15 slightly increases. The minimum at H17 is almost constant at the three different intensities. In the pressure dependence, we notice an evolution of the spectral shape mainly at maximum at H13, increasing from a backing pressure of 1.5 bar to the higher gas pressures, and at H15 which decreases for increasing backing pressure. The intensities of the H21 and above show also a decrease with increasing pressure mainly due to the increase of the Ar intensities with pressure (the SF_6 intensities being quite flat).

From the RABBIT scans, we extracted the emission times. Figure 3 a,b) show the emission times in HHG -defined as the spectral derivative of the spectral phase $\partial\Phi/\partial\omega$- for the same data sets as in Figure 2 (solid lines for SF_6 and dashed lines for argon). In our experiment we have access to the absolute value of the emission time with respect to the phase of the generation field.[25] This absolute emission time allows direct comparison between the two gases without any arbitrary offset of the emission time, e.g., emission time fixed at one sideband. It is extracted from the oscillations of the total HHG yield caused by the overlap of the generation and the dressing fields in the generation medium. Depending on their delay, the electric fields constructively or destructively interfere and therefore modulate the total harmonic signal with a frequency of ω, as observed in the RABBIT scan in Figure 2a). In all measurements we find that the emission times in SF_6 are globally shifted by an offset of approximately -150 as with respect to the corresponding Ar reference. In Figure 3, the measured emission times in Ar show a clear linear spectral dependence with a slope that decreases with increasing intensity. This has been explained by the group delay dispersion (GDD, defined as the spectral derivative of the emission time $\partial t_e/\partial\omega$) associated with the atto-chirp of the continuum electron wavepacket.[22] This intrinsic GDD is inversely proportional to the driving laser intensity. As above mentioned, we also use this dependency to calibrate the laser intensity in the generation medium. The emission time difference between to neighboring harmonics, i.e., the above slope or constant GDD,

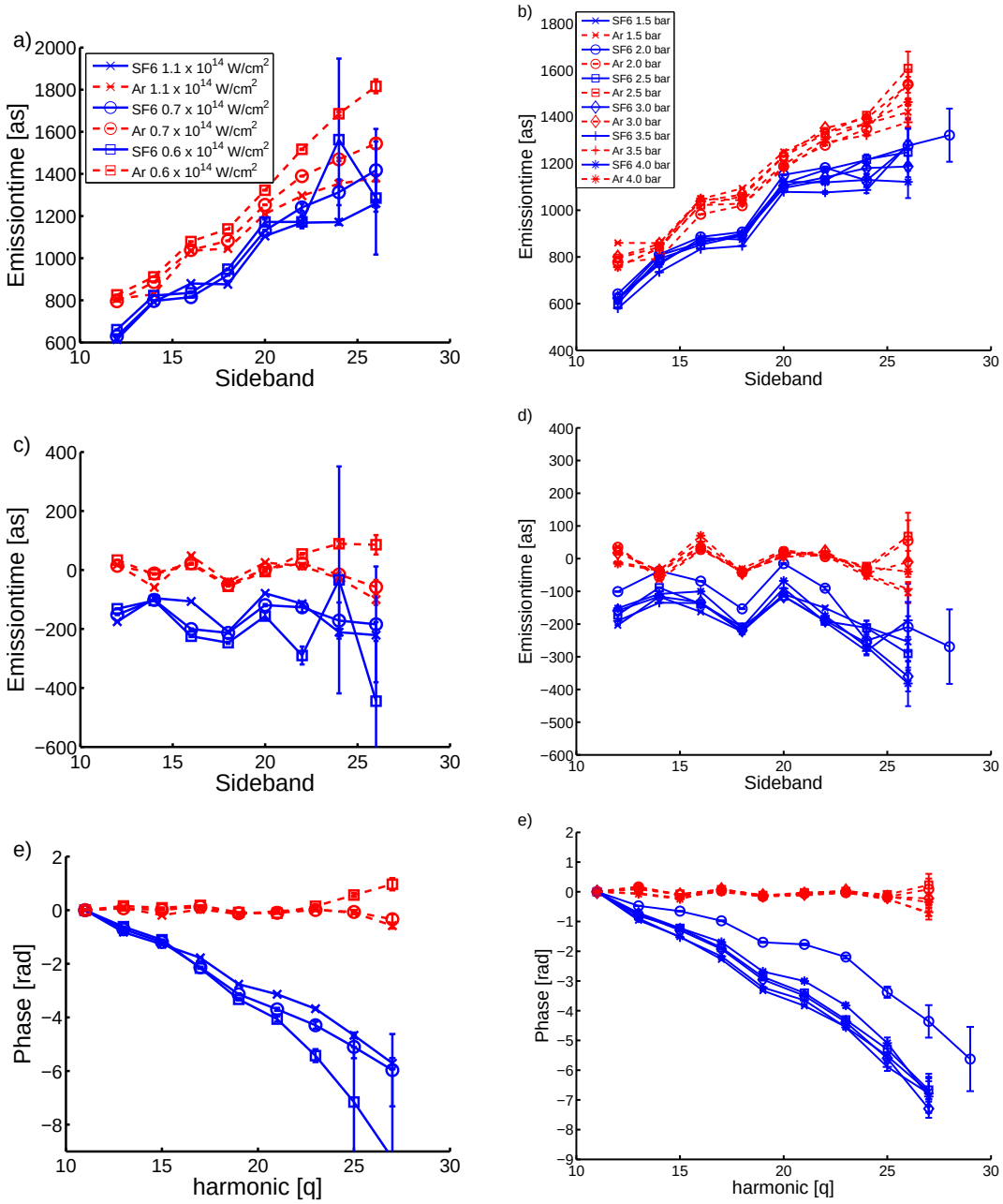

Figure 3: High harmonic emission times of SF_6 (solid line) and Ar (dashed line) for a) three laser intensities from 0.6×10^{14} Wcm^{-2} to 1.1×10^{14} Wcm^{-2} at 3 bar backing pressure and b) for six backing gas pressure from 1.5 bar to 4 bar at 1.1×10^{14} Wcm^{-2} c,d) Difference between the measured emission times for SF_6 and Ar and the linear fit to the argon emission times for the three intensities shown in a) and the six pressures shown in b). e,f) The spectral phase calculated from the emission time differences shown in c,d) The errorbars are given by the strength of the amplitude oscillation at $2\omega_0$ relative to the noise level of the Fourier transformation over the delay dependence of each SB. The error is smaller than the symbol size for the low SBs and becomes very large for the highest SBs due to the low signal to noise ratio for these.

was derived from the measured emission times of the Ar reference, using a linear least square fit, see Table 1.

Table 1: intrinsic GDD of the Harmonic emission of Ar extracted from the RABBIT measurements and corresponding generation intensities

Laser intensity [10^{14}W/cm^2]	GDD [as/3.1 eV]
0.6	134
0.7	117
1.1	99

After removing the intrinsic GDD, using a linear calibration, from the SF_6 data, we obtain the corrected emission times shown in Figure 3 c) and d). By using a linear calibration instead of the measured "true" emission times in Ar, we avoid singularities in the Ar HHG emission, e.g. the autoionizing resonance close to H17,[26] which slightly affects the emission time of SB18. After the calibration only the variation of the spectral phase caused by the molecular influence of SF_6 is remaining. In SF_6 we find a systematic deviation in the emission time from that with constant GDD at the SB16 and SB18 close to the spectral minimum at H17. The deviation is small but very reproducible, around -100 as compared to emission times at SB14 and SB20. When changing the generation intensity, the emission time at SB18 remains unchanged, whereas that at SB16 vanishes for a generation intensity of 1.1×10^{14} Wcm^{-2}. From the calibrated emission times we can retrieve by a simple integration the spectral phase of the recombination dipole in HHG, shown in Figure 3 e). The phases are all normalized to zero at H11. The intensity dependent emission time at SB16 leads to a small phase deviation at H17, at the position where we also observe the minimum in the spectral intensity. Figure 3 d) and f) show the calibrated emission times and the corresponding spectral phase for the different backing gas pressures 1.5 to 4 bar at an intensity of 1.1×10^{14} Wcm^{-2}. It emphasizes the emission time deviation mainly at SB18 for this intensity and the general drop of the spectral phase. The SF_6 emission time at 1 bar backing pressure does not follow the same trend as all the other measurements; we attribute this to a larger uncertainty in this particular RABBIT scan. All the other SF_6 measurements are very similar. The values

for the SB26 and SB28 fluctuate noticeably with large error bars due to the low signal to noise ratio. There is no significant pressure dependence of the measured emission times.

To summarize the main experimental results: the high harmonic emission in SF_6 is much less efficient -by a factor 50 at the same generation intensity- than the emission in Ar. HHG shows simultaneously two features, a clear spectral minimum and a deviation of -100 as in the emission time close to H17. These features are observed for all generation intensities and for backing gas pressures; they are slightly intensity dependent and independent of the backing gas pressure. Additionally, we measure an overall -150 as shift of the emission times in SF_6 with respect to those in Ar. In the following we discuss possible reasons for these experimental trends.

4 Macroscopic response and phase matching

The maximum macroscopic HHG emission occurs in the forward direction of the driving laser beam because of phase matching between the laser-induced nonlinear polarization and the XUV field, leading to the coherent addition of microscopic emissions. This phase matching is usually spectrally dependent, so that the macroscopic HHG spectrum may be strongly modified from the single atomic or molecular emission.[27] The main parameters for phase matching in HHG are the slip of the laser geometrical phase in the focal region, the laser spectral phase dispersion caused by the neutral gas and the free electrons produced by ionization, and the intrinsic dipole phase variation.[28] By appropriately choosing the focus position with respect to the jet, the gas density and the generation intensity, a good phase matching can be achieved over the whole spectral range. Moreover, the reabsorption of the harmonic radiation also determines the macroscopic response, all the more important as the pressure is high.

Constant et al have investigated the conditions for maximum HHG in gases.[29] They show that the highest conversion efficiency is achieved for a coherence length $L_{coh} > 5L_{abs}$

with L_{abs} the absorption length of the XUV light in the gas medium and a medium length $L_{med} > 3L_{abs}$. The XUV flux saturates for $L_{med} > 6L_{abs}$. In this absorption limited HHG, the amplitude at the harmonic order q is proportional to

$$D_{HHG}^{macro}(q) \propto \left| \frac{d_{rec}(q)}{\sigma(q)} \right| \tag{1}$$

the recombination dipole d_{rec} divided by the absorption cross section σ. Now the absorption cross section can be estimated as the modulus square of the photoionization dipole, or equivalently the recombination dipole. The amplitude in the case of absorption limited HHG is therefore given by

$$D_{HHG}^{macro}(q) \propto \left| \frac{1}{d_{rec}(q)} \right| \tag{2}$$

From this result follows that, in the absorption limited HHG, the spectral shape is strongly altered with respect to the microscopic response given by the Lewenstein model, where $D_{HHG}(q)$ is proportional to $d_{rec}(q)$, see equation Equation 3.[30] A large recombination dipole of the sample atoms or molecules would not lead to a large HHG signal but to a small one and vice versa. This is the reason of the large HHG emission around 50 eV in argon when generating in absorption limited conditions provided by a gas-filled hollow-core fiber.[31–33] Indeed, the Cooper minimum at this photon energy strongly decreases the absorption cross section to only 0.7 Mbarn.

As we are interested in the HHG response from the single atom or molecule, we have to verify that our measurements are robust against changes in the macroscopic conditions. The easiest way is to change the gas density in the jet. We were using a pulsed expansion of the gas through a hole with 200 µm diameter with an electronic opening time of the piezo valve for 130 µs. The interaction region of the gas with the laser focus was as close as possible to the nozzle, i.e., approximately 0.4 mm downstream, with a medium length of $\approx 300\mu$m. For estimating the gas density in the center of the interaction region we applied the formalism by David R. Miller describing the free jet expansion of an ideal gas.[34] At 20 °C and 3 bar

backing pressure we calculated a density of $5 \times 10^{17}\text{cm}^{-3}$ for SF_6 and for Ar $2 \times 10^{18}\text{cm}^{-3}$ in the center of the jet. The absorption length of the XUV light at the maximum of the photoionization cross section is 150 µm for SF_6 and 140 µm for Ar at these gas densities.

This is of the same order as the effective length of the interaction volume in the gas jet, therefore we might have absorption effects in the HHG. Figure 2 d) showed that the pressure dependences are very flat for all orders in SF_6 except for H15 that shows a clear decreasing trend. And this is precisely at this spectral position that a strong absorption cross section of 70 Mbarn has been measured (see Section 6). In Ar, the pressure dependences are flat for the low orders, and slightly increasing for the orders H21 and higher (factor 2 over the investigated range). Moreover, the emission times measured in Ar show the behavior expected for the single atom response. Therefore, we reliably assume that influence of the reabsorption on the spectral shape and the phase of the harmonic emission can be neglected in both Ar and SF_6, except for maybe H15 in SF_6.

The offset we observed between the SF_6 and Ar emission times might also result from a macroscopic effect due to different phase matching of the harmonic radiation in the two different gases. Similar effects were already observed in Ar,[35] in that case the emissiontime offset should be pressure dependent. In our experiment we changed the backing gas pressure from 1.5 bar to 4 bar, that is molecule density in the gas jet by a factor of 2.6: still there is no significant change in the measured emission time offset. We conclude therefore that this emission time offset is also an effect coming from the different microscopic response of SF_6 and Ar.

In the following, we develop two models for interpreting the experimental results, based on two distinct assumptions on the single molecule level, respectively, the dominant role of molecular structure in the multi-center, single-channel description of ionization in Section 5, and the dominant role or dynamics in the multi-channel description of ionization in Section 6.

5 Single-channel microscopic response: Multi-center interference model

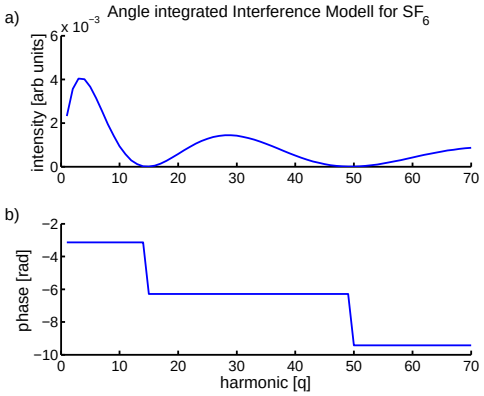

Figure 4: Calculated Harmonic spectral intensity (a) and phase (b) using the multi-center interference model. Two intensity minima with corresponding π phase jumps are visible at the harmonic orders 15 (23.25 eV) and 49 (76.0 eV).

In the first description, we assume that HHG in SF_6 results from a single ionization channel, corresponding to the field ionization of the HOMO orbital and production of the $SF_6{}^+$ ion in the ground state. According to the quantum mechanical version of the 3-step model, the amplitude of the q-th harmonic order emitted by a single molecule can be approximately written as the product of three complex amplitudes,[30,36] describing the tunnel ionization $\gamma_{\mathbf{ion}}$, the continuum propagation $\mathbf{a_{cont}}$ and the recombination $\mathbf{d_{rec}}$ of the electron wave packet with the ion.

$$\mathbf{D}_{HHG}(q,\theta,\varphi) = \gamma_{\mathbf{ion}}(q,\theta,\varphi) \times \mathbf{a_{cont}}(q) \times \mathbf{d_{rec}}(q,\theta,\varphi) \tag{3}$$

Here, θ and φ are the (polar, azimuthal) angular spherical coordinates of the D6-symmetry molecular axis in the frame, where the laser polarization is the polar (z) axis. According to the standard assumptions of the strong field approximation (SFA),[30] we assume, for a given generation intensity, that i) the continuum amplitude $\mathbf{a_{cont}}$ associated to the propagation of the EWP is independent of the ion properties and the molecular alignment and ii) that

the spectral dependance for the tunnel ionization amplitude $\gamma_{\mathbf{ion}}^{\mathrm{SF_6}}(q,\theta,\varphi)$ of SF_6 is the same as that of $\gamma_{\mathbf{ion}}^{\mathbf{Ar}}(q)$ of Ar, since both gases have the same ionization potential. Moreover we only consider the microscopic response, that is we neglect here the role of macroscopic phase matching. Under these assumptions, in the expression of the spectral intensity ratio between SF_6 and Ar three factors are removed, the spectral response of the detection system, the continuum propagation amplitude $\mathbf{a_{cont}}$ of the HHG process and the spectral component of the tunnel ionization amplitude $\gamma_{\mathbf{ion}}^{\mathrm{Ar}}$.

$$\frac{\left|\mathbf{D}_{\mathrm{SF_6}}(q,\theta,\varphi)\right|^2}{\left|\mathbf{D}_{\mathrm{Ar}}(q)\right|^2} = \left|\frac{\gamma_{\mathbf{ion}}^{\mathrm{SF_6}}(q,\theta,\varphi)\times\mathbf{a_{cont}}(q)\times\mathbf{d}_{\mathbf{rec}}^{\mathrm{SF_6}}(q,\theta,\varphi)}{\gamma_{\mathbf{ion}}^{\mathrm{Ar}}(q)\times\mathbf{a_{cont}}(q)\times\mathbf{d}_{\mathbf{rec}}^{\mathrm{Ar}}(q)}\right|^2 \tag{4}$$

As the SF_6 molecular frame cannot be fixed in the experiments, we can only extract the single molecule response integrated over all possible molecular orientations from the experimental data:

$$\frac{\left|\mathbf{D}_{\mathrm{SF_6}}(q)\right|^2}{\left|\mathbf{D}_{\mathrm{Ar}}(q)\right|^2}\times\left|\mathbf{d}_{\mathbf{rec}}^{\mathrm{Ar}}(q)\right|^2 = \left|\int\gamma_{\mathbf{ion}}^{\mathrm{SF_6}}(\theta,\varphi)\times\mathbf{d}_{\mathbf{rec}}^{\mathrm{SF_6}}(q,\theta,\varphi)\,d\theta d\varphi\right|^2 \tag{5}$$

Finally we have to multiply the intensity ratio with the square modulus of the recombination dipole moment $\left|\mathbf{d}_{\mathbf{rec}}^{\mathrm{Ar}}(q)\right|^2$, i.e., the argon photoionization cross section well known from synchrotron experiments,[26] to correct for the spectral response of the Ar reference. Finally we retrieve this way the calibrated spectral intensity, which depends only on the molecule under investigation, from the measurements. These experimental trends are shown in Figure 2 e) and f).

To explain, at least partially, the features of the high harmonic emission from aligned linear molecules a simple model based on interferences in the scattering of the recollinding electron wave packet by a two-center molecule has been proposed, as a typical case of structural interference.[37–39] In the following, we generalize this two-center model into a multi-center interference model. As a first assumption, we describe the recolliding EWP as a plane wave of momentum $\mathbf{k}$. The EWP scattering by the molecular ion is reduced to the interaction with n point-like centers, respectively located at the positions $\mathbf{r}_j$ of the n atoms

j in the molecule. For a given $\mathbf{k}$, i.e., XUV photon energy E_{HHG}, the XUV field amplitude A resulting from the n-center scattering therefore expresses as:

$$A = \sum_{j=1}^{n} A_j \exp\left(i\mathbf{k}(\mathbf{r} - \mathbf{r}_j) + i\phi_j\right) \tag{6}$$

The modulus of the EWP momentum $\mathbf{k}$ is calculated from the XUV photon energy without taking into account the ionization potential of the molecule:[11]

$$|\mathbf{k}| = \frac{2\pi}{h}\sqrt{2mE_{HHG}} \tag{7}$$

This allows a first-order correction for the coulomb field of the ion, which accelerates the incoming EWP before the scattering interaction, whether this correction is justified is still under debate. The phase ϕ_j in Equation 6 corresponds to the scattering phase of the EWP by the different centers, as it can be calculated in, e.g. the Hartree-Fock description of the molecular orbitals. The three degenerate highest occupied molecular orbital (HOMO) of SF_6 are obtained as a combination of the four p-orbitals localized at the fluorine atoms in, respectively, the x-y, x-z and y-z planes. The HOMO orbital in the x-y plane is shown in Table 2. Each HOMO is anti-symmetric with respect to the center of the molecule. The calculation of the XUV field amplitude is made for each degenerate orbital separately and the results are added up coherently. The resulting amplitude of the XUV field in Equation 6, is finally numerically integrated in spherical coordinates over the azimuthal angle Θ from 0° to 360° in 1° steps and for the polar angle φ from 0 to 180° also in 1° steps in order to take into account the isotropic angular distribution of SF_6.

The resulting spectral intensity and phase of the XUV field are shown in Figure 4 a) and b). Two very pronounced minima are visible in the intensity at the harmonic orders 15 and 49, they are connected to sharp π- jumps in the spectral phase. This could thus be an explanation for the minimum observed at H17 in the measured harmonic spectrum (such a simple model cannot be expected to provide the exact position of structural interferences

without hand designed, system specific, correction, i.e the first-order correction of the ionic coulomb field). We do not claim that the minimum can be fully interpreted by the 6-center interference minimum, but our model suggests that the structure of the SF_6 orbitals may be surprisingly important even in the unaligned gas sample.

An experimental check of the second minimum at H49 (photon energy of 76 eV) in the HHG spectrum of SF_6 was not possible with the Ti:Sa PLFA laser system. We are not able to generate harmonic orders above H27 in SF_6 due to ionization saturation of the medium. In a collaboration with the Friedrich Schiller University, we were able to perform some measurements in this high spectral range using a laser system based on optical parametric amplification.[40] The laser delivers pulses of 6.5 fs duration at 950 nm wavelength, which allows extending the high harmonic cut off in SF_6 and Ar to 100 eV. The minimum at 76 eV predicted by the multi-center interference model for SF_6 was not observed in these measurements. As an intermediate conclusion, although the multi-center scattering model accounts for spectral features, maximum and minimum respectively at H13 and H17, it predicts extra ones which are not measured. Multi-center scattering should take place in SF_6 but should not be the dominant process which accounts for HHG properties.

6 Multi-channel microscopic response: dynamical interferences

For rare-gas atoms the dominant contribution to HHG is that of the highest ionization channel due to the exponential decrease of the tunnel ionization rate with increasing binding energy of the electron. In molecules, this general dependence is affected by the fact that different valence states have a much smaller difference in binding energy, and by the non-spherical symmetry of the molecular orbitals. These two features can lead to significant contributions of inner valence states as already evidenced for N_2, CO_2 and N_2O.[10,11] The SF_6 molecule in his ground state has six valence (monoelectronic states) orbitals within 7

eV below the ionization threshold, the $1t_{1g}$ orbital being the HOMO; their symmetry and ionization potentials are listed in Table 2. The HOMO is the $1t_{1g}$ state. In addition, we have to consider that, in our spectral range, two shape resonances are known from photoionization experiments.[41] They result from dipole allowed transitions from the u-symmetry molecular orbitals to the t_{2g} continuum orbital at +5.0 eV and to the e_g continuum orbital at +15.2 eV. Both involve continuum orbitals with grade symmetry and are therefore not dipole coupled to the $1t_{1g}$ HOMO, but to the $5t_{1u}$ HOMO-1 at a binding energy of 16.9 eV and the $1t_{2u}$ HOMO-2 at a binding energy of 17.3 eV. We are therefore expecting to observe an effect of these resonances around 22 eV and 32 eV photon energy, which correspond approximately to the H15 and H21, but only when these lower valence orbitals are contributing significantly to the HHG

Table 2: The SF_6 valence monoelectronic states with their Hartree-Fock orbitals and the experimental binding potentials.[41]

	State	HF Orbital	Ip [eV]		State	HF Orbital	Ip [eV]
X	$1t_{1g}$	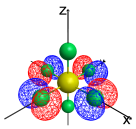	15.7	A	$5t_{1u}$	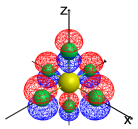	16.9
B	$1t_{2u}$	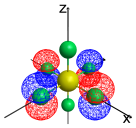	17.3	C	$3e_g$	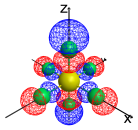	18.6
D	$1t_{2g}$	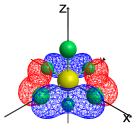	19.7	E	$4t_{1u}$	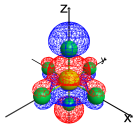	22.5

One very prominent feature in our measurements is the difference of approximately 150 as in the absolute emission times between the HHG in SF_6 and Ar, shown in Figure 3 c and d). This offset transforms into the linear drop of the spectral phase for the SF_6 harmonic emission, shown in Figure 3 e) and f). A possible explanation is the dominant contribution of

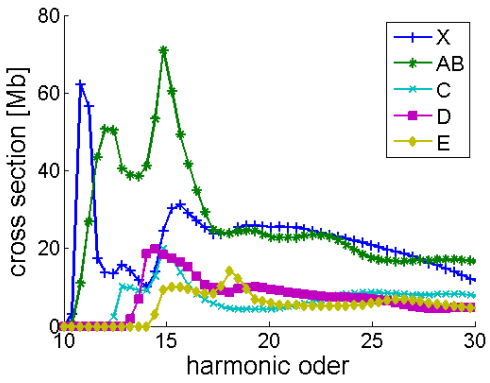

Figure 5: The experimental photoionization cross sections for the different ionization channels of SF_6 [41]

deeper valence orbitals to HHG. The photon energy in HHG is the sum of the kinetic energy of the recolliding EWP and the binding energy of the contributing atomic or molecular orbital. Accordingly, recombination to a lower lying bound orbital will shift the photon energy by the difference ΔI_p in binding energy. In the SFA model, the influence of the ion on the free electron is neglected so that a specific emission time is uniquely related to the kinetic energy of the recollinding EWP. Thus harmonics emitted by the lower-lying bound states will have emission times shifted down by ΔI_p multiplied by the intrinsic GDD. The contribution from an inner valence orbital will reduce the emission times for all harmonic orders and increase the spectral cut-off. Following this argument we can explain the observed emission time differences using the GDD values given in Table 1 by dominant emission from an inner valence orbital with an I_p close to 19.7 eV for all three generation intensities; that is exactly the ionization threshold of SF_6 in the D channel. As the SF_6 molecule has six outer valence orbitals, the assumption of a dominant single, especially an inner one, contribution, might be too much simplifying. Instead we should consider the contributions of all valence orbitals, as shown by recent calculations and experiments, which emphasize strong contributions of the inner valence orbitals to HHG in SF_6. [21]

We model the emission of the q-th harmonic order by the coherent superposition of the uncoupled contributions of the six highest valence orbitals, similar to the approach used by

Diveki et al for HHG in N_2.[42] Each channel k is described within the SFA model[30,36] by its complex tunnel ionization amplitude $\gamma_{ion}^k \times e^{i\phi_{tun}^k}$, the continuum propagation phase factor of the EWP $e^{i\phi_c^k(q)}$ and the recombination dipole moment complex amplitude $d_{rec}^k(q) \times e^{i\phi_{rec}^k(q)}$.

$$D_{HHG}(q) = \sum_{k=1}^{6} \gamma_{ion}^k \times e^{i\phi_{tun}^k} \times e^{i\phi_c^k(q)} \times d_{rec}^k(q) \times e^{i\phi_{rec}^k(q)} \tag{8}$$

The molecular orbitals have a very complex structure, which should significantly affect the tunnel ionization rates compared to the atomic ADK ionization rates.[43] We treat these ionization rates and their phases as unknowns in the calculation. Tunnel ionization rates are in general de-correlated from the final HHG photon energy, so they are assumed constant for each ionization channel. The phase ϕ_c^k that the electron acquires during its continuum propagation can be calculated for each state from the SFA model for the corresponding binding potential, neglecting the influence of the molecular potential and describing the EWP as a plane wave in this step. The EWP amplitude in the continuum propagation is constant in the plateau of the HHG spectrum and decrease exponentially in the cutoff.[42] As the cutoff starts above H25 in our experimental conditions the assumption of a constant EWP amplitude is reasonable. The EWP recombination and the subsequent emission of a XUV photon is the inverse process of the photo ionization, except for the presence of the laser electric field in this step. Ignoring it to a first approximation, the modulus of the recombination dipole can be calculated as $d_{rec}^k(q) = \sqrt{\sigma^k(q)}$ from the photoionization cross section σ^k for the different ionization channels. The cross sections σ^k are known from synchrotron measurements[41,44] or can be calculated using different approximations.[45,46] Noticeably, the agreement between the published experimental and theoretical values is not very good in our spectral range from 15 eV to 45 eV. Depending on the cross section values we use, the results of our calculation change significantly. In the experimental cross sections the A and B ionization channels of SF_6 are almost degenerate and only a combined cross section can be extracted from the data.[41] In our simulation we used this combined cross section, which we refer to as AB ionization channel in the following, see Figure 5. The

last quantities required are the spectral phases $\phi^k_{rec}(q)$ of the recombination dipole for each molecular orbital. To the best of our knowledge no theoretical calculations of the spectral phase of the photoionization matrix elements of SF_6 has been published so far. Therefore, through this approximation may be oversimplifying considering the several resonances in SF_6, we assume $\phi^k_{rec}(q)$ to be independent of the harmonic order. The two unknown phases in the model, the phase of the recombination dipole moment and the tunnel ionization phase, are combined into a channel specific phase. In summary, the two adjustable parameters are the ionization amplitude of each ionization channel and the phase of the specific ionization channel.

An additional factor which might be important are nuclear dynamics occuring in the remaining ion during the EWP continuum excursion, affecting both the amplitude and the phase of the harmonic signal.[47] It was recently shown to be a non negligible factor even for a molecule with "heavy" nuclei such as N_2.[42] Accounting for this factor requires to compute the nuclear autocorrelation function[48] in the ion, between the ionization and recombination times. While it is trivial for diatomic molecules, this represents a considerable computational task for larger molecules with many nuclear degrees of freedom as SF_6. It is not accounted for in the results presented above. In a preliminary test, we have however computed the autocorrelation function by considering a single active coordinate, namely the dissociation of $SF_6{}^+$ in its electronic ground state into $SF_5{}^+$ and F along one of the S-F bonds.[49] The results suggest that the nuclear motion does not affect significantly the harmonic signal (amplitude and phase) in the present case, but more elaborate simulations are further needed to consolidate that assumption.

From our experimental results, we retrieve the complex HHG amplitude $D_{HHG}(q)$ and compare it to the theoretical amplitude calculated from the superposition of the ionization channels. We use a least-square fit procedure to obtain the "adjustable" parameters -the channel specific phase and the tunnel ionization amplitude- for each of the ionization channels X, AB, C, D and E. The result is shown in Figure 6 for the two intensities 0.7×10^{14} Wcm^{-2}

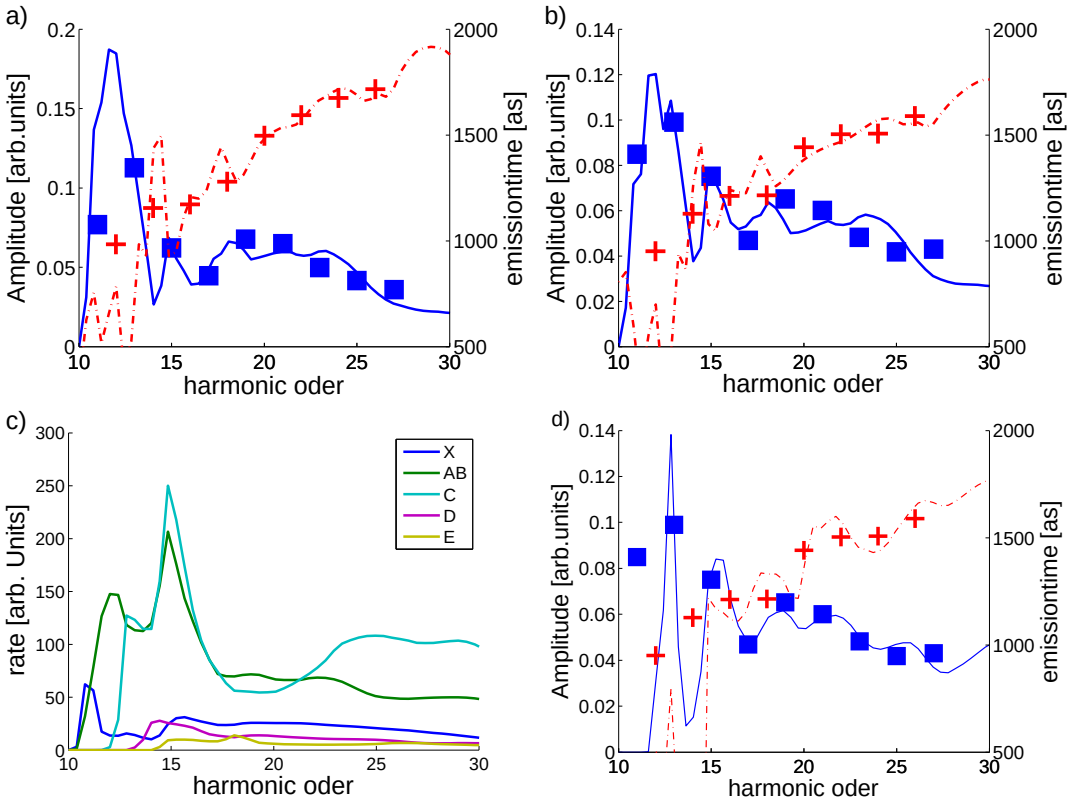

Figure 6: Comparison of the calculated HHG amplitude (solid) and emission times (dashed) for the superposition of the X, A, C, D and E ionization channels of SF_6 and the measured spectral amplitude (■) and emission time (+) for a generation intensity of 0.7×10^{14}W/cm^2 (a) and 1.1×10^{14}W/cm^2 (b). c) The HHG rate (tunnel ionization rate × photorecombination rate) resulting from the least square fit procedure for the X, A, B, C, D and E ionization channels at a generation intensity of 1.1×10^{14} Wcm^{-2}. The photorecombination rate is taken from synchrotron measurements[41] d) Comparison of the experimental data with the calculated HHG amplitude and emission time for a generation intensity of 1.1×10^{14} Wcm^{-2} using calculated photorecombination crosssections[45]

and 1.1×10^{14} Wcm^{-2}. The agreement between the measured and calculated amplitudes is quite good for both measurements. The maximum at H13 and the minimum at H17 are roughly reproduced. The experimental and computed data agrees nicely up to H27. In both calculated spectra additional features are visible in the calculated amplitudes in the range from the H11 to H15. We could not resolve these small structures in the experimental data: our spectral sampling, given by the position of the harmonic lines, is too coarse. The HHG emission time extracted from the calculation is also shown in Figure 6 a) and b). The calculated emission time is around 1100 as for SB12, which is about 330 as higher than the one measured in the Ar and about 470 as higher than the one measured in SF_6. This is apparently a systematic error between the SFA simulation and the RABBIT experiments even for the simple atomic generation gas like argon. For the comparison with the theory, we shifted the measured emission times by 330 as, so that they match the calculated ones in Ar. After correction the measured group delay shift of 150 as between SF_6 and Ar is reproduced in the multi-orbital calculation. Above SB18 the emission times increase linearly as expected due to the atto-chirp; the experimental and theoretical values match very nicely. Below SB18 the overall trend of the experimental emission times is reproduced. The calculation show many sharp features, which are connected to the sharp minima in the calculated HHG amplitude, but these features are too sharp to be resolved in our experiment.

The extracted factors for tunnel ionization rates and channel specific phases are listed in Table 3. The strongest contribution is from the C channel and the AB channel. This agrees well with recent experimental findings and tunnel ionization rate calculations,[21] which also predict a strong contribution from the C and A channels in SF_6. Figure 6 c) shows the contributions of the different ionization channels to HHG (photorecombination rates multiplied by the tunnel ionization rate) at a generation intensity of 1.1×10^{14} Wcm^{-2}. Since the tunnel ionization rate is larger, but the photoionization cross section lower, for the C channel than for the AB channel, their final contributions to the high harmonic generation are similar. The maxima of both ionization channels are at H15, but they are out

Table 3: ionization rates and channel specific phases used in the multichannel HHG calculation equation (6), a) when using the experimental ionization cross-section for SF_6,[41] b) when using the theoretical ionization crosssections for SF_6.[45]

a)

Generation intensity	0.7×10^{14}W/cm^2		1.1×10^{14}W/cm^2	
Ionization channel	tunnel ionization rate [arb.units]	ion.channel phase [rad]	tunnel ionization rate [arb.units]	ion.channel phase [rad]
X $1t_{1g}$	1	0	1	0
AB $5t_{1u}$/ $1t_{2u}$	3.0	-0.6	2.9	-1.0
C $3e_g$	10.6	-0.9	12.5	-1.4
D $1t_{2g}$	1.1	-0.8	1.4	-1.4
E $4t_{1u}$	0.8	0.9	1.0	0

b)

Generation intensity	0.7×10^{14}W/cm^2		1.1×10^{14}W/cm^2	
Ionization channel	tunnel ionization rate [arb.units]	ion.channel phase [rad]	tunnel ionization rate [arb.units]	ion.channel phase [rad]
X $1t_{1g}$	1	0	1	0
A $5t_{1u}$	13	0	25	-0.2
B $1t_{2u}$	7.7	-2.4	14	-2.7
C $3e_g$	0.3	-0.7	1	-1.0
D $1t_{2g}$	1.7	-1.7	7.5	-2.2
E $4t_{1u}$	0.2	2.7	0.0	1.7

of phase by 2.5 rad at this harmonic order (total phase difference is the sum of the continuum plus the channel specific phase differences), so that their contributions cancels each other approximately. The observed minimum at H17 can be explained by a destructive interference between the three main contributing X, AB and C channels. The phase difference between the X and AB channels and between the AB and C channels is almost exactly π at H17 for both generation intensities; this also means that the X and C channel are constructively interfering.

As above mentioned, we have to point out that these calculated contributions and phases for the different ionization channels depend dramatically on the photoionization cross section used. We repeated the previous calculation, but using the calculated cross sections by Yang et al.[45] which noticeably differ from the ones measured in by Holland et al.[41] We also could find a good fit of the data, but leading to different adjustable quantities, ionization rate in k channel and channel specific phases, see Figure 6 d) and Table 3 b). In this description, the

ionization channels A and B dominate HHG whereas the other channels have significantly smaller contribution. This absence of the C channel is in contradiction with the result presented by Ferré et al.[21]

In all calculations the contribution from the HOMO is small, this seems to confirm that the geometry of the HOMO orbital, with its many nodal planes and opposite lobe orientations, drastically reduces the tunnel ionization probability, so that HHG is dominated by the contribution of lower valence orbitals.

7 Conclusion

We have presented a detailed study of the high harmonic generation driven in SF_6 molecules in the gas phase by 800 nm wavelength laser pulses. The HHG emission is completely characterized in spectral intensity and phase over a broad spectral range of up to 40 eV using RABBIT technique. The overall HHG yield in SF_6 is much lower than in argon under similar generation conditions, which we attribute to a reduced tunnel ionization probability of the SF_6 molecule. The involved molecular orbitals have many nodal planes, whose reduce on average the tunnel ionization rate of the molecule. We observed two main features in the calibrated spectral intensity and phase of the XUV emission, at the harmonic order 13 we observed a maximum and at the Harmonic 17 (photon energy of 26.35 eV) a minimum and a corresponding deviation in the measured emission time are reported. In addition the HHG emission times in SF_6 show a vertical offset compared to the emission times of the Ar reference. These features are independent of the backing gas pressure but depends slightly on the generation laser intensity.

We successively investigated two possible interpretations of the results on the basis of two theoretical modellings, first, a multi-center scattering of the recolliding electron by the SF_6 octahedral molecular structure, and second, the contribution of multiple ionization channels to HHG. Both descriptions lead to a spectral minimum around the H17. However, the multi-

center scattering model based on plane waves predicts a sharp π phase jump at H17, which is not found in the experimental spectral phase. This model also predicts a second minimum at H50, which was not found in complementary measurements done with an IR, few cycle OPCPA laser source. The multi-channel contribution model unambiguously leads to a better agreement with the experimental results. Two main features, the maximum at H13 and the minimum at H17 and the emission times deviation around H17, are well reproduced. The model can also explain the -150 as offset between the SF_6 emission times and the Ar reference without assuming unrealistic high contributions of inner valence orbitals to HHG. Our analysis allows the extraction of tunnel ionization rates for the different contributing molecular orbitals. The contribution from the HOMO is suppressed, the main contributions come from deeper valence orbitals HOMO-3, HOMO-1 and HOMO-2. This is in good agreement with a recently reported experiment, but the retrieved values dependent strongly on the selected recombination cross section.

Although this model could reproduce remarkably well our experimental findings, the input for the modeling has to be significantly improved. In particular one should consider the spectral dependence of the phase of the recombination dipole. The amplitude of the recombination dipole can be extracted from photoionization experiments, but the spectral phase is not yet accessible in these experiments. We assumed it to be constant over the whole spectral range, which is questionable since several well-known resonances lie this range; they will have certainly an effect on the spectral phase of the recombination dipole. Finally, we assumed independent channels but they could be coupled by the laser field, resulting in additional coupled channels that could play a role in the total emission.

Our study illustrates the richness of the data encoded in HHG and the difficulties of interpreting them in a self-probing picture. More specifically, the "structural" and "multi-channel" origin of the observed interferences are often opposed against each other, while they rather should be considered jointly, since they are not incompatible. Further theoretical and experimental work is needed to uncover the rich physics underlying HHG from SF_6

molecules. Of particular interest would be the study of HHG driven by a mid-IR source, where the longer wavelength allows a finer sampling of the resonance region in the different ionization channels, as well as measurements in an extended spectral range.

8 Acknowledgment

The authors are particularly grateful to Jean-Michel Mestdagh and collaborators who, in the eighties, have introduced at CEA-Saclay the principles and techniques of time-resolved studies in physical-chemistry. Since then, their diffusion from femtochemistry to attophysics at CEA-Saclay ought in first rank to the scientific merits and ideas, talent for teaching and making deep subtle things accessible, constant interest for nonlinear optics and the potential of coherent pulses in the XUV range, that Jean-Michel Mestdagh has marked over years and brought to his colleagues.

The authors are also indebted to Dr. Jean-François Hergott and Fabien Lepetit who very efficiently operated the PLFA laser at the Saclay Laser-Matter Interaction Center (CEA-SLIC).

This work was supported by the FP7 program LASERLAB-EUROPE, Grant No. 284464, ITN-ATTOFEL and IEF-AttoDynamics; the French National Research Agency (ANR) through the "Laboratoire d'Excellence Physics Atoms Light Mater" (ANR-10-LABX-0039-PALM) and ATTOWAVE project (ANR-09-BLAN-0031-01). J.R. acknowledges support by the german academic exchange service (DAAD).

9 References

References

(1) McPherson, A.; Gibson, G.; Jara, H.; Johann, U.; Luk, T. S.; McIntyre, I. A.; Boyer, K.; Rhodes, C. K. Studies of multiphoton production of vacuum-ultraviolet radiation in the

rare gases. *J. Opt. Soc. Am. B* **1987**, ***4***, 595.

(2) Sarukura, N.; Hata, K.; Adachi, T.; Nodomi, R.; Watanabe, M.; Watanabe, S. Coherent soft X-ray generation by the harmonics of an ultrahigh-power KrF laser. *Phys. Rev. A* **1991**, *43*, 1669.

(3) Paul, P. M.; Toma, E. S.; Breger, P.; Mullot, G.; Augé, F.; Balcou, P.; Muller, H. G.; Agostini, P. Observation of a train of attosecond pulses from high harmonic generation. *Science* **2001**, *292*, 1689.

(4) Hentschel, M.; Kienberger, R.; Spielmann, C.; Reider, G. A.; Milosevic, N.; Brabec, T.; Corkum, P.; Heinzmannß, U.; Drescher, M.; Krausz, F. Attosecond metrology. *Nature* **2001**, *414*, 509.

(5) Krausz, F.; Ivanov, M. Attosecond physics. *Reviews of Modern Physics* **2009**, *81*, 163–234.

(6) Corkum, P. B. Plasma perspective on strong-field multiphoton ionization. *Physical Review Letters* **1993**, ***71***, 1994.

(7) Schafer, K. J.; Yang, B.; DiMauro, L. F.; Kulander, K. C. Above threshold ionization beyond the high harmonic cutoff. *Phys. Rev. Lett.* **1993**, ***70***, 1599.

(8) Seres, J.; Seres, E.; J.Verhoef, A.; Tempea, G.; Streli, C.; P.Wobrauschek,; Yakovlev, V.; Scrinzi, A.; Spielmann, C.; Krausz, F. Source of coherent kiloelectronvolt X-rays. *Nature* **2005**, *433*, 596.

(9) Popmintchev, T.; Chen, M.-C.; Popmintchev, D.; Arpin, P.; Brown, S.; Ališauskas, S.; Andriukaitis, G.; Balčiunas, T.; Mücke, O. D.; Pugzlys, A. et al. Bright Coherent Ultrahigh Harmonics in the keV X-ray Regime from Mid-Infrared Femtosecond Lasers. *Science* **2012**, *336*, 1287–1291.

(10) Smirnova, O.; Mairesse, Y.; Patchkovskii, S.; Dudovich, N.; Villeneuve, D.; Corkum, P.; Ivanov, M. Y. High harmonic interferometry of multi-electron dynamics in molecules. *NATURE* **2009**, *460*, 972–977.

(11) Haessler, S.; Caillat, J.; Boutu, W.; Giovanetti-Teixeira, C.; Ruchon, T.; Auguste, T.; Diveki, Z.; Breger, P.; Maquet, A.; Carre, B. et al. Attosecond imaging of molecular electronic wavepackets. *Nature Physics* **2010**, *advance online publication*.

(12) Kanai, T.; Minemoto, S.; Sakai, H. Quantum interference during high-order harmonic generation from aligned molecules. *Nature* **2005**, *435*, 470.

(13) Wagner, N. L.; Wüest, A.; Christov, I. P.; Popmintchev, T.; Zhou, X.; Murnane, M. M.; Kapteyn, H. C. Monitoring molecular dynamics using coherent electrons from high harmonic generation. *Proc. Nat. Ac. Sci. USA* **2006**, *103*, 13279–13285.

(14) Wörner, H.; Bertrand, J.; Kartashov, D.; Corkum, P.; Villeneuve, D. Following a chemical reaction using high-harmonic spectroscop. *Nature* **2010**, *466*, 604–607.

(15) Wörner, H.; Bertrand, J.; Fabre, B.; Higuet, J.; Ruf, H.; Dubrouil, A.; Patchkovskii, S.; Spanner, M.; Mairesse, Y.; Blanchet, V. et al. Conical intersection dynamics in NO2 probed by homodyne high-harmonic spectroscopy. *Science* **2011**, *334*, 208–212.

(16) Vozzi, C.; Calegari, F.; Benedetti, E.; Berlasso, R.; Sansone, G.; Stagira, S.; Nisoli, M.; Altucci, C.; Velotta, R.; Torres, R. et al. Probing two-centre interference in molecular high harmonic generation. *Journal of Physics B: Atomic, Molecular and Optical Physics* **2006**, *39*, S457.

(17) Levesque, J.; Mairesse, Y.; Dudovich, N.; Pepin, H.; Kieffer, J.-C.; Corkum, P. B.; Villeneuve, D. M. Polarization State of High-Order Harmonic Emission from Aligned Molecules. *Physical Review Letters* **2007**, *99*, 243001.

(18) Mairesse, Y.; Higuet, J.; Dudovich, N.; Shafir, D.; Fabre, B.; Mével, E.; Constant, E.; Patchkovskii, S.; Walters, Z.; Ivanov, M. Y. et al. High Harmonic Spectroscopy of Multichannel Dynamics in Strong-Field Ionization. *Physical Review Letters* **2010**, *104*, 213601.

(19) Itatani, J.; Levesque, J.; Zeidler, D.; Niikura, H.; Pépin, H.; Kieffer, J. C.; Corkum, P. B.; Villeneuve, D. M. Tomographic imaging of molecular orbitals. *Nature* **2004**, *432*, 867.

(20) Vozzi, C.; Negro, M.; Calegari, F.; Sansone, G.; Nisoli, M.; De Silvestri, S.; Stagira, S. Generalized molecular orbital tomography. *Nature Physics* **2011**, *7*, 822–826.

(21) Ferré, A.; Boguslavskiy, A.; Dagan, M.; Blanchet, V.; Bruner, B.; Burgy, F.; Camper, A.; Descamps, D.; Fabre, B.; Fedorov, N. et al. Multi-channel Electronic and Vibrational Dynamics in Polyatomic High-order Harmonic Generation. *arXiv preprint arXiv:1407.6213* **2014**,

(22) Mairesse, Y.; de Bohan, A.; Frasinski, L. J.; Merdji, H.; Dinu, L. C.; Monchicourt, P.; Breger, P.; Kovačev, M.; Taïeb, R.; Carré, B. et al. Attosecond synchronization of high-harmonic soft X-rays. *Science* **2003**, *302*, 1540.

(23) Mauritsson, J.; Gaarde, M. B.; Schafer, K. J. Accessing properties of electron wave packets generated by attosecond pulse trains through time-dependent calculations. *Phys. Rev. A* **2005**, *72*, 013401.

(24) Weber, S. J.; Manschwetus, B.; Billon, M.; Böttcher, M.; Bougeard, M.; Breger, P.; Géléoc, M.; Gruson, V.; Huetz, A.; Lin, N. et al. Flexible attosecond beamline for high harmonic spectroscopy and XUV-IR pump probe experiments requiring long acquisition times. *Review of Scientific Instruments* **2014**, submitted.

(25) Dinu, L. C.; Muller, H. G.; Kazamias, S.; Mullot, G.; Augé, F.; Balcou, P.; Paul, P. M.;

Kovačev, M.; Breger, P.; Agostini, P. Measurement of the Subcycle Timing of Attosecond XUV Bursts in High-Harmonic Generation. *Phys. Rev. Lett.* **2003**, ***91***, 063901.

(26) Samson, J.; Stolte, W. Precision measurements of the total photoionization cross sections of He, Ne, Ar, Kr, and Xe. *Journal of Electron Spectroscopy and Related Phenomena* **2002**, 265–276.

(27) Schnürer, M.; Cheng, Z.; Hentschel, M.; Tempea, G.; Kálmán, P.; Brabec, T.; Krausz, F. Absorption-Limited Generation of Coherent Ultrashort Soft-X-Ray Pulses. *Phys. Rev. Lett.* **1999**, *83*, 722.

(28) Kazamias, S.; Daboussi, S.; Guilbaud, O.; Cassou, K.; Ros, D.; Cros, B.; Maynard, G. Pressure-induced phase matching in high-order harmonic generation. *Phys. Rev. A* **2011**, *83*.

(29) Constant, E.; Garzella, D.; Breger, P.; Mével, E.; Dorrer, C.; Blanc, C. L.; Salin, F.; Agostini, P. Optimizing High Harmonic Generation in Absorbing Gases: Model and Experiment. *Physical Review Letters* **1999**, *82*, 1668.

(30) Lewenstein, M.; Balcou, P.; Ivanov, M.; L'Huillier, A.; Corkum, P. B. Theory of high-order harmonic generation by low-frequency laser fields. *Phys. Rev. A* **1994**, *49*, 2117.

(31) III, C. G. D.; Rundquist, A. R.; Backus, S.; Herne, C.; Murnane, M. M.; Kapteyn, H. C. Phase matching of high-order harmonics in hollow waveguides. *Phys. Rev. Lett.* **1999**, *83*, 2187.

(32) Tamaki, Y.; Nagata, Y.; Nagata, Y.; Obara, M.; Midorikawa, K. Phase-matched high-order harmonic generation in a gas-filled hollow fibre. *Physical Review A* **1999**, *59*, 4041.

(33) Rothhardt, J.; Hädrich, S.; Demmler, S.; Krebs, M.; Fritzsche, S.; Limpert, J.; Tün-

nermann, A. Enhancing the Macroscopic Yield of Narrow-Band High-Order Harmonic Generation by Fano Resonances. *Physical review letters* **2014**, *112*, 233002.

(34) Miller, D. R. *Free jet sources*; Oxford University Press: New York, 1988; Vol. 1.

(35) Kroon, D.; Guénot, D.; Kotur, M.; Balogh, E.; Larsen, E.; Heyl, C.; Miranda, M.; Gisselbrecht, M.; Mauritsson, J.; Johnsson, P. et al. Attosecond pulse walk-off in high-order harmonic generation. *Optics letters* **2014**, *39*, 2218–2221.

(36) Le, A.-T.; Lucchese, R.; Tonzani, S.; Morishita, T.; Lin, C. Quantitative rescattering theory for high-order harmonic generation from molecules. *Physical Review A* **2009**, *80*, 013401.

(37) Lein, M.; Hay, N.; Velotta, R.; Marangos, J.; Knight, P. Interference effects in high-order harmonic generation with molecules. *Physical Review A* **2002**, *66*, 023805.

(38) Vozzi, C.; Calegari, F.; Benedetti, E.; Caumes, J.-P.; Sansone, G.; Stagira, S.; Nisoli, M.; Torres, R.; Heesel, E.; Kajumba, N. et al. Controlling two-center interference in molecular high harmonic generation. *Physical Review Letters* **2005**, *95*, 153902.

(39) Lock, R. M.; Zhou, X.; Li, W.; Murnane, M. M.; Kapteyn, H. C. Measuring the intensity and phase of high-order harmonic emission from aligned molecules. *Chemical Physics* **2009**, *366*, 22 – 32, Attosecond Molecular Dynamics.

(40) Rothhardt, J.; Demmler, S.; Hädrich, S.; Limpert, J.; Tünnermann, A. Octave-spanning OPCPA system delivering CEP-stable few-cycle pulses and 22 W of average power at 1 MHz repetition rate. *Opt. Express* **2012**, *20*, 10870–10878.

(41) Holland, D.; MacDonald, M.; Baltzer, P.; Karlsson, L.; Lundqvist, M.; Wannberg, B.; Von Niessen, W. An experimental and theoretical study of the valence shell photoelectron spectrum of sulphur hexafluoride. *Chemical Physics* **1995**, *192*, 333–353.

(42) Diveki, Z.; Camper, A.; Haessler, S.; Auguste, T.; Ruchon, T.; Carré, B.; Salières, P.; Guichard, R.; Caillat, J.; Maquet, A. et al. Spectrally resolved multi-channel contributions to the harmonic emission in N 2. *New Journal of Physics* **2012**, *14*, 023062.

(43) Tong, X. M.; Zhao, Z. X.; Lin, C. D. Theory of molecular tunneling ionization. *Physical Review A* **2002**, *66*, 033402.

(44) Addison Jones, B.; Tan, K.; Bancroft, G.; Cerrina, F. A comparison of shape resonant behavior in the inner-shell photoabsorption and valence-level photoelectron spectra of sulfur hexafluoride, sulfur chloride fluoride and selenium hexafluoride (SF6, SF5Cl and SeF6). *Chemical Physics Letters* **1986**, *129*, 468–474.

(45) Yang, L.; Ågren, H.; Carravetta, V.; Vahtras, O.; Karlsson, L.; Wannberg, B.; Holland, D.; MacDonald, M. Energy-dependent valence photoelectron spectra of SF6. Ab initio calculations and measurements. *Journal of Electron Spectroscopy and Related Phenomena* **1998**, *94*, 163 – 179.

(46) Jose, J.; Lucchese, R.; Rescigno, T. Interchannel coupling effects in the valence photoionization of SF6. *The Journal of Chemical Physics* **2014**, *140*, 204305.

(47) Haessler, S.; Boutu, W.; Stankiewicz, M.; Frasinski, L. J.; Weber, S.; Caillat, J.; Taieb, R.; Maquet, A.; Breger, P.; Monchicourt, P. et al. Attosecond chirp-encoded dynamics of light nuclei. *Journal of Physics B: Atomic, Molecular and Optical Physics* **2009**, *42*, 134002, International Conference on Multi-Photon Processes, Heidelberg, GERMANY, 2008.

(48) Lein, M. Attosecond Probing of Vibrational Dynamics with High-Harmonic Generation. *Phys. Rev. Lett.* **2005**, *94*, 053004.

(49) Tachikawa, H. Ab initio MO calculations of structures and electronic states of SF6 and SF6. *Journal of Physics B: Atomic, Molecular and Optical Physics* **2002**, *35*, 55.

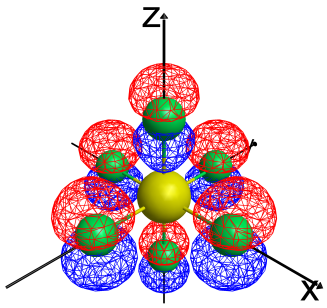

Figure 7: TOC graphic